CFD Modelling of Arctic Coastal Erosion due to Breaking Waves

Nadeem Ahmad*[1], Hans Bihs[1], Mayilvahanan Alagan Chella[1], Arun Kamath[1], and Øivind A. Arntsen[1]

[1]Department of Civil and Environmental Engineering, Norwegian University of Science and Technology (NTNU), 7491 Trondheim, Norway

International Journal of Offshore and Polar Engineering, 2019, **29** (1), pp. 33-41.
DOI: http://dx.doi.org/10.17736/ijope.2019.ak31

Abstract

This paper presents the numerical modelling of the seawall erosion due to the wave impact on a vertical seawall. The open-source CFD model REEF3D is used for the modelling. The model solves the Reynolds-Averaged Navier-Stokes equations along with the k-ω model and morphological model. The waves are generated in the numerical wave tank using the relaxation method. The free surface and the change in the bed profile are captured with the level set method. The simulated hydrodynamics and the beach profiles are compared with the experimental data. Results discuss the beach profile development for different case scenarios of the seawall locations, the wave steepness, and the beach slopes.

Keywords: Wave breaking; Coastal erosion; Free surface; Breaking wave; Seawall; Arctic coastline; Large-scale CFD; REEF3D.

1 Introduction

The seawalls are used to protect the beach erosion due the excessive sediments transport in seaward direction during the severe waves condition. However, the wave impact on the seawall aggravates from the seawall toe, which threatens the stability of the seawall. The design decisions and scour mitigation strategies are considered rather challenging as the complex nature of the waves and the coastline together with the high cost of the construction of

*Corresponding author,nadeem.ahmad@ntnu.no

Postprint, published in International Journal of Offshore and Polar Engineering, doi:http://dx.doi.org/10.17736/ijope.2019.ak31

the scour remedy measures are involved. The physical process of erosion at the coastline is defined as follows: wave breaking near the bed results in higher bed shear stresses around the breaking point. An increase in the bed shear stress compared to the critical shear stress initiates sediment pickup and wave-induced current transport sediment away (Sumer et al., 2002). Further, if the bluff or a seawall obstructs the coastline, the wave impact creates an undertow current. It mobilises the sediments from the toe, which are then carried offshore by the near-bed current. The process continues until the scour hole at the toe is deep enough to dissipate the wave impact (Fredsøe and Deigaard, 1992).

The experimental investigations of the seawall erosion have received considerable attention in the past decade (Dean, 1987; Hughes and Fowler, 1990; Fowler, 1992; Kamphuis et al., 1992; Kraus and Smith, 1994; Kraus and McDougal, 1996; Sumer et al., 2001; Sutherland et al., 2006; Tsai et al., 2009). Huge and Fowler (Hughes and Fowler, 1990; Fowler, 1992) conducted midscale experiments using the suitable scaling relationships appropriate for modeling wave-induced erosion in a small-scale model. The results of reproduced cross-shore profiles were compared with the prototype-scale tests and showed a close match. Kamphuis et al. (1992) investigated the seawall scour for the three-dimensional movable bed. The oblique random waves were generated on a sloping profile (1:10) and the change in beach profile for different wave heights was discussed. Kraus and Smith (1994) conducted a series of the experiments to investigate the seawall scour for the wave heights ranging from 0.4 to 1 m. The experiments were performed in a large-scale model and the detailed analysis is carried out for the longshore, cross-shore sediment transport, the seawall toe erosion and the seawall failure case under the severe storm conditions. It was concluded that presence of the seawall majorly affects the immediate beach profile, however the majority of the beach profile remains the same which existed before a seawall in place. Among the recent studies, Sutherland et al. (2006) performed the experiments for the seawall erosion. Test were conducted for the vertical and an inclined seawall (1:2) placed on the mild beach slope ranging from 1 in 30 to 75 by imposing the waves of significant wave height varying from 0.1 to 0.2. It is concluded that the maximum scour depth depends on the relative water depth at the seawall toe and wave similarity parameter (ξ_0). In addition, the results demonstrated that the seawall erosion seems insensitive to the slope of the seawall, where an inclined seawall reproduced the similar scour depths as a vertical seawall. Tsai et al. (2009) investigated the experimental results of the toe scour of seawall on a steep seabed with slope of m=1:5 under the action of breaking waves. The equilibrium toe scour profiles were investigated and the depths of toe scours related to the wave parameters were analysed. Experimental observation indicated that the depth of toe scour increases with the steepness of the incoming wave, but decreases with an increase in the water depth at the seawall toe.

The development of a numerical model for sediment transport due to wave action is a challenging task, and only limited progress has been made in this area e.g. Bihs and Olsen (2011); Ahmad et al. (2015); Afzal et al. (2015); Ahmad et al. (2016); **?**. In these studies, flow hydrodynamics around the coastal structure such as piles, pipeline and abutments, is obtained by solving the Navier-Stokes equations coupled with sediment algorithms to predict the maximum scour depth. Dally and Dean (1984) and Dally et al. (1985) are among the first to attempt numerical modelling of coastline sediment transport. They developed a mathematical model for beach profile evolution. Roelvink and Stive (1989) investigated the formation of the cross-shore profile under irregular waves. It is found that wave asymmetry leads to the formation of a breaker bar towards the beach, while the undertow current

initiates the offshore movement of the breaker bar. McDougal et al. (1996) developed a numerical model for coastal erosion. Unlike the previous numerical models where the waves in the breaking zone were dissipated in an ad-hoc manner, their model included the reflected waves from the seawall. It is found that the profile responses to a storm for a beach with and without a seawall are relatively similar, except close to the wall. Dronen and Deigaard (2007) developed a morphological quasi three-dimensional numerical model for a barred coastline. Gislason et al. (2009) investigated the numerical modelling of the standing waves and scour in front of breakwaters. Zou et al. (2012) investigated the case of wave breaking and seawall toe scour in front of a vertical wall placed on a mild slope by solving the Reynolds Averaged Navier-Stokes Solver (RANS) combined with a Volume of Fluid (VOF) method for the free surface capturing. However, the calculation of the free surface capturing is not compared with the experimental data. One of the most recent study on coastline erosion processes is from Jacobsen and Fredsøe (2014), where the breaking wave hydrodynamics and the sediment transport over a morphologically fixed bed with a constant slope are discussed. Results of the transport rate are presented in terms of the surf similarity and Dean's parameter. Finally, the morphological development of the cross-shore profile is determined.

This paper will describe the numerical modelling of seawall erosion with the sharp free surface capturing due to the wave impact on the seawall. A validated model for the breaking waves kinematics for the spilling and the plunging breaker (Alagan Chella et al., 2015, 2016) is applied to simulate the erosion at the seawall toe. Results discuss the wave kinematics on the steep slope (m=1:4) with a vertical seawall place in. The wave propagation over the slope, the location of the breaking wave, the wave asymmetry, change in the velocity profiles are captured with the level ste method and the development of the beach profiles is simulated using the Exner's formulation incorporates bed-load sediment transport equations. The results of the wave hydrodynamics and the change in the profile are compared with a discussed for the breaking waves, formation of standing waves and the wave impacts on the seawall; the significant contributors to a beach profile change. The numerical results are found in agreement with experimental data produced by Hughes and Fowler (1990). The numerical results further revealed the change in beach profile for different case scenarios of the seawall locations, the incident wave heights, and the seabed slopes.

2 NUMERICAL MODEL

The CFD modelling of erosion due to the wave impact is carried out using the open-source numerical model REEF3D. The numerical model has been successfully used for the investigation of breaking waves, the interaction of breaking waves with coastal structures and numerical modelling of sediment transport Bihs et al. (2016); Alagan Chella et al. (2016); Bihs and Kamath (2017); **?** by solving the mathematical equations of the flow and the sediment transport which are briefly discussed below:

2.1 Hydrodynamic Model

It solves the incompressible Reynolds-Averaged Navier-Stokes (RANS) equations, along with the continuity equation to calculate the velocity field in the numerical wave tank (NWT). The

continuity and momentum equations are shown below:

$$\frac{\partial u_i}{\partial x_i} = 0 \tag{1}$$

$$\frac{\partial u_i}{\partial t} + u_j \frac{\partial u_i}{\partial x_j} = -\frac{1}{\rho}\frac{\partial p}{\partial x_i} + \frac{\partial}{\partial x_j}\left[(\nu + \nu_t)\left(\frac{\partial u_i}{\partial x_j} + \frac{\partial u_j}{\partial x_i}\right)\right] + g_i \tag{2}$$

where u_i is the fluid velocity, t is the time, p is the pressure, ρ is the density of water, ν is the kinematic viscosity of the water, ν_t is the eddy viscosity and g is the gravitational acceleration.

The $k-\omega$ model (Wilcox, 1994) is used to calculate the turbulence parameter, eddy viscosity (ν_t) is obtained by solving the two variables namely, the turbulent kinetic energy k and the specific turbulent dissipation ω. The free surface is captured using the level set method (Osher and Sethian, 1988). It uses a continuous signed distance function to represent the interface between two immiscible fluids. The details of the turbulence model and level set method implemented in this numerical model can be found in Bihs et al. (2016).

2.2 Morphological model

The simulated flow field from the hydrodynamic model is used to simulate the sediment transport process where the hydrodynamic change after each hydrodynamic time step is coupled with the morphological model. The morphological process is simulated as follows:

Bed shear stress and bed load calculation The bed shear stress on the bed is calculated using the hydraulically rough wall function. The bed shear velocity near the bed is determined by considering the logarithmic velocity profile. The calculation of the bed shear stress τ is defined as follows:

$$\tau = \rho u_*^2 \tag{3}$$

where u_* is the bed shear velocity and defined as:

$$\frac{u}{u_*} = \frac{1}{\kappa}\, ln\left(\frac{30.2z}{k_s}\right) \tag{4}$$

where u is the water velocity, u_* is the shear velocity, $\kappa = 0.40$ is the von Karman constant, z is the vertical height above the seabed to nearest cell center, $k_s = 3d_{50}$ is the Nikuradse's equivalent sand roughness, d_{50} is the median grain size. The bed load calculations are made with the formulation proposed by van Rijn (1984). It is based on the sediment particle mobility, which suggests that when the bed shear stress just exceeds the critical bed shear stress, the motion of the sediment is initiated and is defined as follows:

$$\frac{q_b}{d_{50}^{1.5}\sqrt{\frac{(\rho_s-\rho_w)g}{\rho_w}}} = 0.053\frac{\left(\frac{\tau-\tau_c}{\tau_c}\right)^{2.1}}{\left(\left(\frac{\rho_s/(\rho_w-1)g}{\nu^2}\right)^{1/3}\right)^{0.3}} \tag{5}$$

where q_b is the bed load transport, τ_c is the critical bed shear stress, ρ_s is the sediment density, ρ_w the water density, g is acceleration due to the gravity, d_{50} is the median particle diameter and ν is the kinematic viscosity of water.

Bed shear stress on slopping bed and morphological evolution The critical bed shear stress calculated using the Shields diagram approach might lead to an underestimation of the sediment transport because it does not account for the effects of a sloping bed. This problem is handled with the modified critical shear formulation on sloping beds proposed by Dey (2003). The effect of a sloping bed is accounted for by considering the longitudinal bed slope θ, the transverse bed slope α, the angle of repose φ and the drag and lift forces. The expression for the bed shear stress reduction factor r is defined as follows:

$$\begin{aligned} r = \frac{1}{\big(1-\eta\tan\varphi\big)\tan\varphi}\Big\{&-\big(\sin\theta+\eta\tan^2\varphi\sqrt{\cos^2\theta-\sin^2\alpha}\big) \\ &+\big[\big(\sin\theta+\eta\tan^2\varphi\sqrt{\cos^2\theta-\sin^2\alpha}\,\big)^2 \\ &+\big(1-\eta^2\tan^2\varphi\big)\big(\cos^2\theta\tan^2\varphi-\sin^2\alpha\tan^2\varphi-\sin^2\theta-\sin^2\alpha\big)\big]^{0.5}\Big\} \end{aligned} \tag{6}$$

where η is the ratio of drag force to inertia force. Finally, the modified critical bed shear stress (τ_c) is calculated by multiplying the Shields critical bed shear stresses τ_0 with the reduction factor r as follows:

$$\tau_c = r \cdot \tau_0 \tag{7}$$

The change in bed elevation is calculated with the Exner formula. The method is based on the conservation of the sediment mass where the spatial variation in the bed load is conserved with the temporal change in the vertical direction. The morphological evolution occurs as a non-linear propagation of the bed level deformations in the direction of the sediment transport. The formulation of the transient change in bed level is given as follows:

$$\frac{\partial z_b}{\partial t} + \frac{1}{(1-n)}\left[\ \frac{\partial q_{b,x}}{\partial x}\ \right] + E - D = 0 \tag{8}$$

where z_b is the bed-level, $q_{b,x}$ is the bed-load in the x direction, n is the sediment porosity, D is the deposition rate, expressed as volume of sediment grain settling and E is the entrainment rate. The term $(E-D)$ defines the net flux of sediment across the interface between the bed load and suspended load and is calculated as suggested by Wu et al. (2000). The transient change in the sediment bed is modelled using the level set method with an implicit representation of the sediment bed as the zero level set. The main advantage of this approach is the consistency and numerical stability with the morphological evolution which does not require re-meshing.

3 NUMERICAL SOLVER

The mathematical equations used in the hydrodynamic and morphological model are approximated using the advanced finite difference methods on a Cartesian grid. The convective terms of the momentum equations are discretized with the fifth-order accurate conservative Weighted Essential Non-Oscillatory (WENO) scheme (Jiang and Shu, 1996) and the convective terms of the turbulence model and the level set function are discretized with the Hamilton-Jacobi formulation of the WENO scheme (Jiang and Peng, 2000). A third-order TVD Runge-Kutta time scheme (Shu and Osher, 1988) is used for time treatment of the momentum equations, the level set function. The hydrodynamic time step for the transient flow

field is determined using adaptive time stepping. In this method, the time step is obtained using the Courant-Friederichs-Lewy (CFL) number (Griebel et al., 1998). The pressure term in the RANS equations is treated with the projection method (Chorin, 1968) to obtain the Poisson equation for pressure and solved using the BiCGStab solver from the high-performance solver package HYPRE with the semi-coarsening multi-grid preconditioner PFMG (Ashby and Flagout, 1996).

4 NUMERICAL SETUP

5 Numerical setup and model validation

The computational setup for the model validation is the same as the one employed by Hughes and Fowler (1990). The NWT is 100 m long with a flat bottom in the beginning from x= 0 to 65 m followed by a sloping seabed of m = 1:4 as shown in Fig. 1. The still water level is h = 0.67 m. The waves of wave height H = 0.20 m and the wave period T = 2.2 s are generated in the NWT. The bed material used for the sloping seabed consists of non-cohesive sand with median particle diameter d_{50} = 0.13 mm. The sediment density is ρ_s = 2700 kg/m^3 and the angle of repose of the sediment is $\varphi = 35°$. The Shields parameter for the bed material is θ_c = 0.047. The sediment bed is assumed to be hydraulically rough with a roughness height of $k_s = 3d_{50}$. The vertical seawall is placed at the intersection of the bed slope and the mean water level. Moreover, the numerical test is run for the profile change under a wave burst of 80 waves. The limitation is due to fact that the bed slope in the experimental set-up consisted of the sand berm laid over the concrete revetment and a wave burst of 80 was allowed to impact on seawall at a time which resulted in the seawall erosion almost exposed to the concrete revetment. A further wave generation incorporated the interference of the concrete revetment on the seawall erosion which is not under the scope of this study. Details of the experimental set-up can be seen in the technical report on midscale physical model validation for scour at coastal structures (Hughes and Fowler, 1990). The boundary conditions of the NWT are as follows: The inlet boundary condition is of Dirichlet type where the incident wave velocity and free surface level are prescribed based on chosen wave theory. The outlet boundary condition is a wall, which is far from the wave breaking and the dissipation zone. The bottom of the NWT is considered as a wall. The two side walls and the top are considered symmetry planes.

6 RESULTS

6.1 Grid and time step size convergence study

At first, a grid size convergence test is carried out. The purpose of the tests is to determine the optimal grid size required to maintain the quality of the waves generated in the 2D NWT. The wave gauge is located at x = 2.0 m, from the inlet. The numerical tests are run with no sediment bed slope in the NWT. Four simulation are run with different of grid size dx = 0.04 m, 0.03 m, 0.02 m and 0.01 m. For all values of the grid size dx, the Courant-Friederichs-Lewy (CFL) criterion is kept to CFL = 0.25. Fig. 1(b) shows the accuracy of the simulated wave through the with the fifth-order cnoidal wave theory. It is found that wave accuracy increases with the decrease in the grid size dx. Fig. 1(c) shows the discrepancy δ

Table 1: The numerical test conditions

Test	dx (m)	CFL	H (m)	T (s)	h (m)	t (s)	S (m)
Grid convergence study							
$A1$	0.04	0.25	0.125	2.00	0.40	25	
$A2$	0.03	0.25	0.125	2.00	0.40	25	
$A3$	0.02	0.25	0.125	2.00	0.40	25	
$A4$	0.01	0.25	0.125	2.00	0.40	25	
Time convergence study							
$B1$	0.01	0.40	0.125	2.00	0.40	25	
$B2$	0.01	0.30	0.125	2.00	0.40	25	
$B3$	0.01	0.20	0.125	2.00	0.40	25	
$B4$	0.01	0.10	0.125	2.00	0.40	25	
Hydrodynamic validation							
$C1$	0.01	0.10	0.125	2.00	0.40	25	
Morphological validation							
$D1$	0.01	0.10	0.20	1.97	1.16	300	0.20
Coastline erosion, Isfjorden							
$E1$	0.01	0.10	3.3	13.3	20.0	300	1.0

between the simulated wave crests, wave troughs, wave phase and wavelength with the wave theory. The calculations of δ are depicted in Fig. 1(c) where δ_{cr} is the discrepancy in wave crests, δ_{tr} is the discrepancy in wave troughs, δ_{ph} is the wave discrepancy in wave phase, $\eta_{max,s}$ is the simulated wave crest, $\eta_{max,t}$ is the theoretical wave crest, $\eta_{min,s}$ is the simulated wave trough, $\eta_{max,t}$ is the theoretical wave trough, $t_{p,s}$ is the simulated wave crest time, $t_{p,s}$ is the theoretical wave crest time, λ_s is the simulated wavelength and λ_t is the theoretical wavelength. The quality of the wave is considered to be good at grid size $dx = 0.01$ m.Fig. 1(d-e) shows the quality of the wave through the time step size convergence study through the profile comparison and the discrepancy between the simulated wave and the wave theory. The optimal grid size from the grid size convergence study $dx = 0.01$ m is maintained. The calculation of transient hydrodynamics is based on an adaptive time stepping where the time step is calculated through the CFL number. Therefore, instead of testing the time step size directly, different values of the CFL number are tested. For this, four different tests with CFL = 0.50, 0.40, 0.30, 0.20 and 0.10 are performed. It is found that the accuracy of the waves increases with a lowering the CFL number and shows a close fit with wave theory for CFL = 0.10. Hence, the solution is considered to be converged at CFL = 0.10 with the grid size dx = 0.01 m.

In order to test the quality of wave generation in the present set-up, a grid convergence study is carried out. The model is tested for a burst of 80 regular waves generated and are impacting then on the seawall. To limit the computational expense, waves are run a shorter domain of $x/\lambda = 6.5$ using the relaxation method. The CFL-number is kept at 0.1. The locations of the wave gauges are chosen as per experimental setup. The probe is located close to point where the slope profile starts as shown in Fig. 1. Four grid sizes of $dx = 0.03$ m, 0.02 m, 0.015 m, and 0.01 m are tested. The results are shown in terms of the wave elevations and are compared with the experiments conducted for the regular wave tests described in (Hughes and Fowler, 1990). It is found the quality of the wave generation is strongly dependent on the grid size dx. Fig. 2(a) shows the simulated wave elevations for $dx = 0.03$ m. The wave troughs show a close fit, However, the wave peaks are significantly low compared to the experimental

data. Figs. 2(b-c) indicate the quality of the wave for the lower grid size of dx= 0.02 m and 0.015 m. The quality of the wave peaks and troughs seem to improve with the lower grid size. Still, the wave peaks in the beginning of the wave generation appear slightly low compared to the experimental data. Fig. 2(d) show the wave elevations for dx = 0.01 m. The simulated wave peaks and troughs show a close fit with experimental data. The solution is assumed to converge at dx = 0.01 m and is considered for the next numerical tests. In addition, the model has already been tested for breaking waves on the spilling and plunging breaker and the detail of the results can be found in the previous papers (Alagan Chella et al., 2015, 2016) .

6.2 Breaking waves on a slope

In this section, the results of wave breaking on a slope are discussed. The purpose of this test is to ensure the quality of the hydrodynamics of the wave propagating and breaking on the slope. The numerical model was previously used to simulate the spilling and plunging breaking waves on a sloping bed (Alagan Chella et al., 2015, 2016). In their study, waves are generated using the relaxation method (Jacobsen et al., 2012). The results showed a good representation of the wave height evolution during the shoaling, breaking and post-breaking. Further, the computed hydrodynamic parameters associated with the breaking process such as free surface elevation, horizontal and vertical components of particle velocity and turbulent kinetic energy were thoroughly analysed and compared with experimental data.

Fig. 1(f) shows the comparison between the numerical and the experimental results for the wave envelope. The upper curve (the red solid line) is the wave envelope representing the simulated wave crest elevations. The waves after t = 10 s are accounted for the wave envelope. It is clearly shown that the wave crests are well captured in the shoaling, incipient breaking and just after the breaking regions. In the surf zone, there is a small difference between the numerical and the experimental wave envelope. This can be explained by the fact that the free surface capturing in the surf zone is a challenging task as the complex intermixing of air and water is involved. The lower curves represent the envelope of the troughs and matches well with the experimental data. Apart from a small discrepancy in the wave crest elevations in the surf zone, the numerical results compare well with the experiment. A detailed study of wave breaking over slope can be found in Alagan Chella et al. (2015) and Alagan Chella et al. (2016).

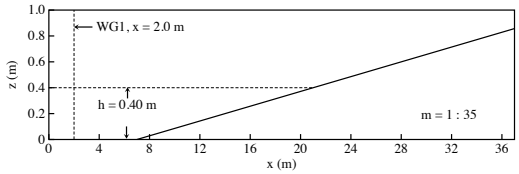

(a) Numerical set-up

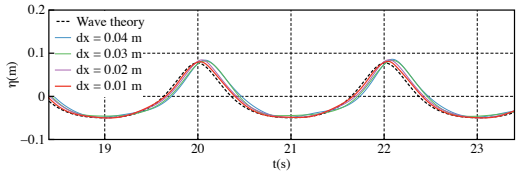

(b) Grid size convergence study. Wave gauge location, $x = 2.0$ m

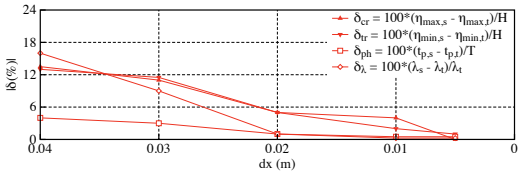

(c) Wave discrepancy against dx. Wave gauge location, $x = 2.0$ m

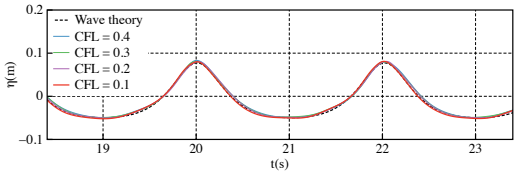

(d) Time step size convergence study

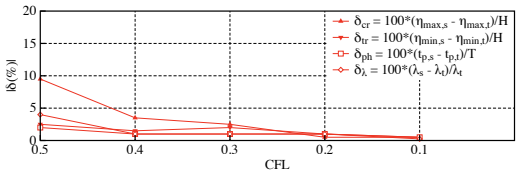

(e) Wave discrepancy against CFL. Wave gauge location, $x = 2.0$ m

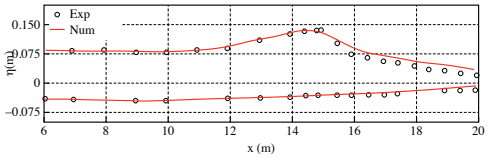

(f) Comparison of simulated and experimental wave envelope

Figure 1: Hydrodynamic validation of the numerical model for the wave breaking on a slope. The red solid line is the numerical results, black dashed line is the wave theory and black circle is the experiment (Ting and Kirby, 1996).

6.3 Seawall erosion validation

The validated numerical model for the wave hydrodynamics on a slope is used to simulate the erosion process. The main focus is on the erosion due to the wave breaking and impact on the vertical bluff. For this, a case study of the seawall erosion is carried out considering the vertical bluff as a seawall. The simulation is run in a 2D NWT which follows the experimental observation from Fowler (1992). The NWT is 100 m long with a flat bottom at the beginning from x= 0 to 65 m followed by a sloping seabed of m = 1:15 as shown in Fig. 2(a). The still water level is h = 1.16 m. The waves with significant wave height H_s = 0.20 m and peak period T_p = 1.97 s are generated in the NWT using the JONSWAP wave spectrum. The seawall is located 0.92 m from the intersection between the still water depth and the bed slope as shown in Fig 2(a). The waves are run for 300 s, which replicates the duration of the irregular waves as used in the experiment. The same spectrum as experiments but different wave realisation is used. The bed slope is provided 30 m away from the wave inlet. The wave gauge is located 8.0 m from the inlet. The bed material used for the sloping seabed consists of non-cohesive sand with the median particle diameter d_{50} = 0.13 mm. The sediment density is ρ_s = 2700 kg/m^3 and the angle of repose of the sediment is $\varphi = 35°$. The Shields parameter for the bed material is θ_c = 0.047. The sediment bed is assumed to be hydraulically rough with a roughness height of $k_s = 3d_{50}$. The seawall is considered as a wall. The other boundary

conditions are the same as discussed in the previous setup. The details of the test case are listed in Table 1.

Fig. 2(b) shows the time series of waves generated using the JONSWAP spectrum. The significant wave height of the waves is $H_s = 0.20$ m and the peak period is $T_p = 1.97$ s. The grid size $dx = 0.01$ m and CFL = 0.10 is used. The gauge is located 10.0 m from the wave inlet and the free surface of the irregular wave is recorded for a duration of T = 300 s. Since, the experimental data for the incident wave time series is not available, a comparison between the numerical and theoretical spectral wave density is made to ensure the quality of the waves as shown in Fig. 2(c). It is found that the spectral peak and spectral wave density show a close fit with the theory for the frequency range $f < 0.5$. This signifies the longer waves are well captured. The numerical result shows slightly lower values for the spectral density function compared to the theory for the frequency range $f > 0.5$. This is probably due to the interaction of shorter waves or small reflections from the slope and the seawall. This small discrepancy is deemed to be acceptable, as the maximum erosion at seawall toe is caused by the longer waves impacting the seawall.

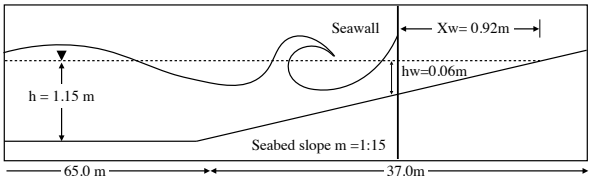

(a) Numerical setup for the seawall erosion.

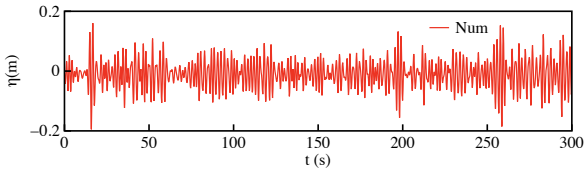

(b) Time series of the incident waves. Wave gauge location, $x = 8.0$ m

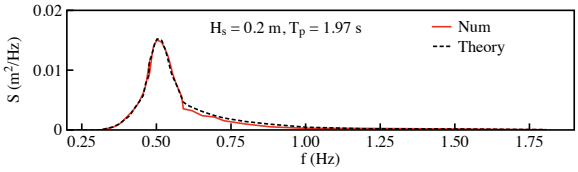

(c) Comparison of the numerical and the theoretical spectral wave density against the wave frequency

Figure 2: The numerical setup and incident wave used for the morphological model validation. Experiment data: Fowler (1992)

Fig. 3(a) shows the sequence of propagation of the irregular waves generated for $t = 300.0$ s and the resulting erosion due to wave breaking and impact on the seawall. The erosion process near the seawall is described in three stages namely the preliminary, intermediate and the final erosion stage. At $t = 30$ s, the preliminary stage of the erosion is depicted. The maximum velocity during the breaking process is 1.9 m/s and the wave breaking point is approximately 1.0 m away from the seawall. A small erosion is seen at this location, which is due to the breaking wave impact. However, there is no erosion at the seawall toe. At $t = 150$ s, the intermediate stage of the erosion process is depicted. This shows a scour hole of depth $S = 0.15$ m near the seawall toe. It is due to the wave impact on the seawall, which creates large velocities acting towards the seawall toe and mobilises the sediments from the toe. The eroded sediments are then carried offshore by the reflected waves and form a breaker

bar. At $t = 300$ s, the final stage of the erosion is depicted. It is seen that the scour hole near the seawall deepens to $S = 0.20$ m. The eroded sediment is deposited offshore and results in a higher breaker bar, which contributes to the shifting of the wave breaking point further offshore. The sequence of this change can be clearly seen at the slope profile between $x = 2.5$ m to 4.5 m. Fig. 3(b) shows the temporal variation of the bed shear stress at the seawall toe.

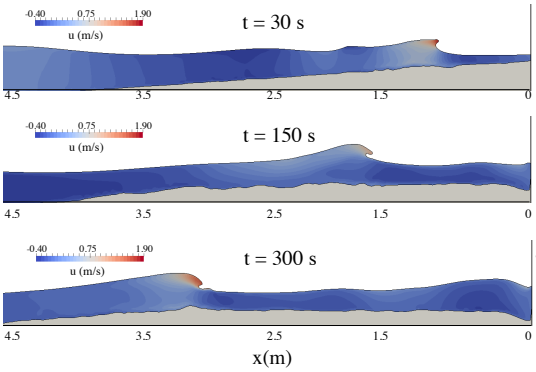

(a) Sequence of the wave breaking and the resulting erosion

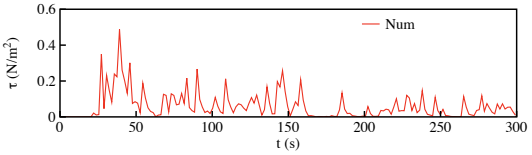

(b) Temporal variation of the bed shear stress at seawall toe

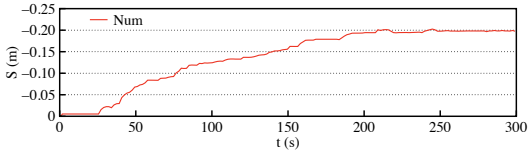

(c) Temporal variation of the maximum erosion at seawall toe

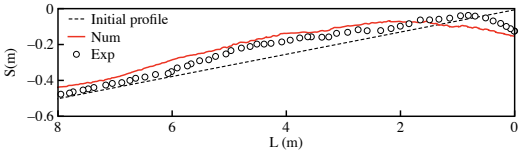

(d) Comparison of the numerical and experimental erosion profile. The bed slope location: 30 m away from inlet, simulation duration: t = 300 s.

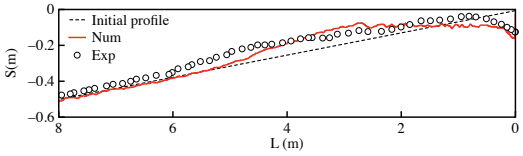

(e) Comparison of the numerical and experimental erosion profile. The bed slope location: 60 m away from the inlet, simulation duration: t = 600 s. Red solid line: numerical profile, dashed lines: initial profile. Experimental data: Fowler (1992)

Figure 3: Validation of the morphological model.

The result shows that the bed shear stress is $\tau = 0$ for t < 35 s; increases to its highest value $\tau = 0.5$ N/m^2 for t = 35 s to t = 150 s and decrease to $\tau = 0.1$ for t > 150 s for the studied wave realisation. This clearly confirms that the maximum bed shear stress at the seawall toe is developed during the first impact of the waves, which results in the maximum erosion in the beginning of the process. Once the scour hole is developed, the bed shear stress starts decreasing with scour depth. This is due to the fact that the momentum transfers from the wave impact on the bed decrease with an increasing scour hole depth at the seawall toe.

Fig. 3(c) shows the temporal variation of the process. It is seen that there is no scour in the beginning as the waves take time to approach the seawall. The maximum erosion takes

place between t = 35 s to t = 150 s. As discussed, this is due to the development of higher bed shear stress during the first wave impact. The change in erosion seems to attain maximum erosion at t = 300 s. Fig. 3(d) shows the comparison of the simulated erosion profile with the experimental data. The simulated maximum erosion at the seawall toe is 0.20 m, which matches the experimental data. The eroded sediment mass is deposited approximately 2.0 m away from the seawall which creates the breaker bar. However, the computed deposition profile is slightly higher than the experimental data. This might be due to the stochastic nature of the waves approaching the seawall and the empirical formulations associated with the morphological model.

Fig. 3(e) depicts simulated scour profile obtained by running a similar simulation with a different wave realisation, increasing the distance between the wave inlet and starting point of bed slope to 60 m and doubling the simulation duration to t = 600 s. The main purpose of this simulation is to ensure that the simulated scour at the seawall toe is independent of the wave realisation, the simulation duration and computation domain length. It is seen that result shows somewhat a different scour profile compared to simulation in a short NWT. However, the scour depth at seawall toe is seen to be the same. This confirms previous findings and contributes additional evidence that suggests the change in the wave realisation might affect the temporal variation. However, the maximum erosion at the seawall toe is expected to be equal to the significant wave height.

6.4 Arctic coastline erosion at Isfjorden, Svalbard

This section presents the investigation of the Isfjorden coastline erosion at Bjørndalen. The sediment properties (Rubensdotter, 2015) of the Arctic coastline are incorporated into the validated model for breaking waves and seawall erosion. Observations showed that major erosion took place at the coast, where gentle slopes end with a vertical bluff. The numerical model is applied to 500 m long cross-shore profile including the vertical bluff and is run for the wave event observed at the Bjørndalen-Isfjorden coastline in September 2015.

A simplified NWT used for the numerical test is shown in Fig. 4(a). The wave characteristics are extracted from the spectral wave model MIKE21 SW (Borgersen, 2016). The significant wave height is calculated to be $H_s = 3.3$ m and the peak period is $T_p = 13.3$ s. The bathymetry data of the Isfjorden coastline is extracted using MIKE C-MAP. The sediment properties for the morphological model are based on the site-specific data for Bjørndalen-Vestpynten, Svalbard where the active sediment layer consists of the glacio-fluvial sand deposits (Rubensdotter, 2015). The Irregular waves are generated using the JONSWAP wave spectrum for a duration of 300 s. The time series of the incident waves is shown in Fig. 4(b). In order to ensure the quality of the incident wave, a comparison between the numerical and theoretical spectral wave density plotted over the frequency of the waves is shown in Fig. 4(c). Results show a good match of the numerical results with the theory which confirms the good quality of the waves propagation in the NWT.

Fig. 4(d) shows the simulated cross-shore profile along with the wave breaking at different time intervals. First, the full seabed profile of L = 500 m long at t = 50 s is shown. The waves shoal approximately 5 m high and overturn in about 3.5 m deep water. In the beginning, this results in no erosion, as the available water depth is deep enough to dissipate the overturned wavefront momentum reaching the seabed. A zoomed-in view of the cross-shore profile of L = 30 m long from the vertical bluff is shown at t = 100 s and t = 150 s. The wave is breaking

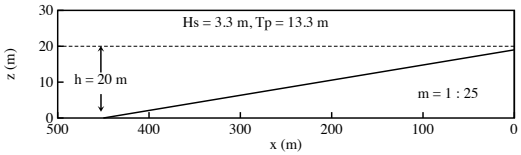

(a) Numerical setup

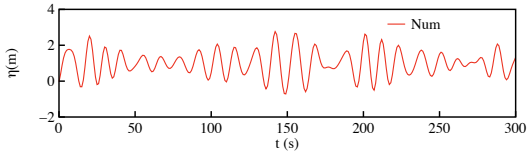

(b) Time series of incident wave. Wave gauge location, $x = 490$ m

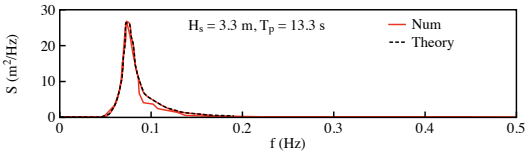

(c) Comparison of the numerical and the theoretical spectral wave density against the wave frequency

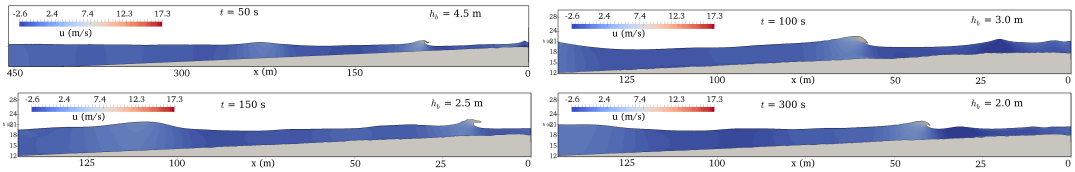

(d) The sequence of the wave breaking and impacting on the vertical bluff

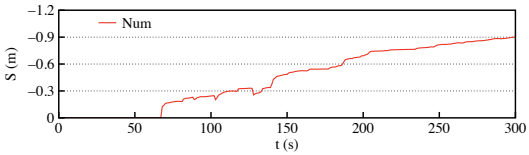

(e) Temporal variation of the erosion process

Figure 4: Simulated wave profiles and the resulting erosion at the Bjørdalen-Isfjorden coastline.

near the coastline with the wave breaking height is varying between 3.0 m and 2.5 m. The maximum wavefront velocities during the overturning process near the bluff toe are found to be between 7.5 to 17.3 m/s, which are large enough to create a strong impact on the seabed and hence contribute substantially to the erosion near the bluff toe. The maximum erosion near the seawall toe after 76 s and 150 s, is seen to be about 0.10 and 0.50 m, respectively. The last figure in the sequence shows the simulated scour profile near the vertical bluff at t = 300 s. The depth of the scour hole near the bluff toe is about 1.0 m deep and the eroded sediment is deposited offshore which forms a breaker bar.

Figs. 4(e) depicts the temporal variation of the maximum erosion at the vertical bluff. It is found that there is no erosion in the beginning and starts after $t = 60$ s. The erosion rate grows rapidly after $t = 60$ s. This is due to the longer waves are approaching and impacting on the vertical bluff, resulting in higher sediment transport from the bluff toe. The maximum erosion is seen to be almost 1.0 m within 300 s. Although the equilibrium scour state is not

achieved, valuable knowledge on the bluff erosion physics for breaking wave impact could be gathered. Despite this limitation, an almost 1.0 m deep scour hole at the vertical bluff is observed within $t = 300$ s of waves. The scour depth is within the range of actual scour depth observed at the Bjørndalen-Isfjorden coastline in September 2015. Therefore, it is an important consideration for the shore protection measures as it influences the characteristics of the waves approaching the shoreline.

7 CONCLUSIONS

This study is a first step towards enhancing the understanding of Arctic coastal erosion for a large domain. The open-source numerical model REEF3D is used to solve the RANS-equations linked with a morphological model. The free surface is captured with the level set method. The numerical model is validated with two different experimental data sets: Ting and Kirby (1996) for breaking wave kinematics and Fowler (1992) for seawall erosion. It is found that the numerical model is suitable for simulating the wave hydrodynamic on a slope and the breaking wave showed a good agreement with the experimental data. A further implementation of the model for the numerical investigation of the sediment transport processes for the maximum scour depth at 300s matches with the experimental observations. It is observed that scouring in the proximity of seawall i.e., the vertical bluff is governed by the wave impact and attains a maximum erosion in short time compared to coastline erosion which is a long-term process. Finally, the numerical model is used to investigate the erosion process at the Bjørndalen-Isfjorden coastline. Results are presented for the temporal variation of the erosion and the eroded coastline line along with the free surface profile. The main conclusions based on the simulated results are as follows:

1. The maximum bed shear stress near the seawall toe is governed by the initial wave impact of the process. The maximum scour depth at 300s matches with the experimental observations, which confirms that erosion in the proximity of the vertical bluff is a short-term process.

2. The simulated erosion and deposition profiles for the seawall erosion match adequately with the experimental observations demonstrating the suitability of the model to predict complex hydrodynamics and resulting erosion process on a vertical bluff under wave impact.

3. The model sufficiently captures the wave hydrodynamics and the resulting erosion for the storm event at the Bjørndalen-Isfjorden coastline in September 2015. The simulated results show that shoaling results in wave height higher than 4.5 m and the maximum erosion of approximately 1 m deep take place at the bluff toe. As an outlook for future research, a longer simulation is needed to determine an equilibrium scour depth in the proximity of the vertical bluff.

4. The eroded sediment deposits offshore and forms a breaker bar which might be an additional cause for the change in the wave breaking pattern.

Acknowledgements

This study has been carried out under the POL- NOR/200336/95/2014 and the authors are grateful to the grants provided by the Research Council of Norway. This study was supported in part with computational resources at the Norwegian University of Science and Technology (NTNU) provided by NOTUR, http://www.notur.no.

References

Afzal, M.S., Bihs, H., Kamath, A. and Arntsen, Ø.A. (2015). Three-dimensional numerical modeling of pier scour under current and waves using level-set method. *Journal of Offshore Mechanics and Arctic Engineering*, **137**(3), 032001.

Ahmad, N., Afzal, S., Bihs, H. and Arntsen, Ø.A. (2015). Three-dimensional numerical modeling of local scour around a non-slender cylinder under varying wave conditions. In: *36th IAHR World Congress, June 2015, The Netherlands*.

Ahmad, N., Bihs, H., Kamath, A. and Arntsen, Ø.A. (2016). 3D numerical modelling of pile scour with free surface profile under wave and current using level set method in model REEF3D. In: *8th International Conference on Local Scour and Erosion, ICSE 2016, Oxford, UK*.

Alagan Chella, M., Bihs, H., Myrhaug, D. and Muskulus, M. (2015). Breaking characteristics and geometric properties of spilling breakers over slopes. *Coastal Engineering*, **95**, 4–19.

Alagan Chella, M., Bihs, H., Myrhaug, D. and Muskulus, M. (2016). Hydrodynamic characteristics and geometric properties of plunging and spilling breakers over impermeable slopes. *Ocean Modelling*, **103**, 53–72.

Ashby, S.F. and Flagout, R.D. (1996). A parallel mulitgrid preconditioned conjugate gradient algorithm for groundwater flow simulations. *Nuclear Science and Engineering*, **124**(1), 145–159.

Bihs, H. and Kamath, A. (2017). A combined level set/ghost cell immersed boundary representation for floating body simulations. *International Journal for Numerical Methods in Fluids*, **83**(12), 905–916.

Bihs, H., Kamath, A., Alagan Chella, M., Aggarwal, A. and Arntsen, Ø.A. (2016). A new level set numerical wave tank with improved density interpolation for complex wave hydrodynamics. *Computers & Fluids*, **140**, 191–208.

Bihs, H. and Olsen, N.R.B. (2011). Numerical modeling of abutment scour with the focus on the incipient motion on sloping beds. *Journal of Hydraulic Engineering*, **137**(10), 1287–1292.

Borgersen, B.T. (2016). *Numerical Modelling of Arctic Coastal Hydrodynamics and Sediment Transport*. Master's thesis, NTNU.

Chorin, A. (1968). Numerical solution of the Navier-Stokes equations. *Mathematics of Computation*, **22**, 745–762.

Dally, W.R. and Dean, R.G. (1984). Suspended sediment transport and beach profile evolution. *Journal of Waterway, Port, Coastal, and Ocean Engineering*, **110**(1), 15–33.

Dally, W.R., Dean, R.G. and Dalrymple, R.A. (1985). Wave height variation across beaches of arbitrary profile. *Journal of Geophysical Research: Oceans*, **90**(C6), 11917–11927. ISSN 2156-2202.

Dean, R.G. (1987). Coastal armoring: effects, principles and mitigation. In: *Coastal Engineering 1986*, 1843–1857.

Dey, S. (2003). Threshold of sediment motion on combined transverse and longitudinal sloping beds. *Journal of Hydraulic Research*, **41**(4), 405–415.

Dronen, N. and Deigaard, R. (2007). Quasi-three-dimensional modelling of the morphology of longshore bars. *Coastal Engineering*, **54**(3), 197–215. ISSN 0378-3839.

Fowler, J.E. (1992). Technical report CERC-92-16: Scour problems and method of prediction of maximum scour at vertical seawalls. Technical report, Department of the Army, Waterways Experiment Station, Corps of Engineers, Vicsburg, Mississippi U.S.

Fredsøe, J. and Deigaard, R. (1992). *Mechanics of coastal sediment transport*, volume 3. World Scientific Publishing Co Inc., *S*ingapore.

Gislason, K., Fredsøe, J. and Sumer, B.M. (2009). Flow under standing waves: Part 2. scour and deposition in front of breakwaters. *Coastal Engineering*, **56**(3), 363 – 370. ISSN 0378-3839.

Griebel, M., Dornseifer, T. and Neunhoeffer, T. (1998). *Numerical simulation in fluid dynamics: a practical introduction*. SIAM.

Hughes, S.A. and Fowler, J.E. (1990). Technical report CERC-90-8: Midscale physical model validation for scour at coastal structures. Technical report, Coastal Engineering Research Center Vicksburg, MS.

Jacobsen, N.G. and Fredsøe, J. (2014). Formation and development of a breaker bar under regular waves. part 2: Sediment transport and morphology. *Coastal Engineering*, **88**, 55 – 68.

Jacobsen, N.G., Fuhrman, D.R. and Fredsøe, J. (2012). A wave generation toolbox for the open-source CFD library: Openfoam. *International Journal for Numerical Methods in Fluids*, **70**(9), 1073–1088.

Jiang, G.S. and Peng, D. (2000). Weighted ENO schemes for Hamilton-Jacobi equations. *SIAM Journal on Scientific Computing*, **21**, 2126–2143.

Jiang, G.S. and Shu, C.W. (1996). Efficient implementation of weighted ENO schemes. *Journal of Computational Physics*, **126**, 202–228.

Kamphuis, J., Rakha, K. and Jui, J. (1992). Hydraulic model experiments on seawalls. In: *Proceedings 23rd Coastal Engineering conference, ASCE*, 1272–1284.

Kraus, N.C. and McDougal, W.G. (1996). The effects of seawalls on the beach: Part i, an updated literature review. *Journal of Coastal Research*, **12**(3), 691–701.

Kraus, N.C. and Smith, J.M. (1994). Supertank laboratory data collection project: Volume i: Main text. *Technical report: CERC-94-3 U.S. Army Engineer Waterways Experiment Station, Coastal Engineering Research centre, Vicksburg, MS.*

McDougal, W.G., Kraus, N.C. and Ajiwibowo, H. (1996). The effects of seawalls on the beach: part ii, numerical modeling of supertank seawall tests. *Journal of Coastal Research*, 702–713.

Osher, S. and Sethian, J.A. (1988). Fronts propagating with curvature-dependent speed: algorithms based on Hamilton-Jacobi formulations. *Journal of Computational Physics*, **79**, 12–49.

Roelvink, J.A. and Stive, M.J.F. (1989). Bar-generating cross-shore flow mechanisms on a beach. *Journal of Geophysical Research: Oceans*, **94**(C4), 4785–4800. ISSN 2156-2202.

Rubensdotter, L. (2015). Landforms and sediments, Bjorndalen-Vestpynten, Svalbard. Technical report : ISBN 978-82-7385-158-1.

Shu, C.W. and Osher, S. (1988). Efficient implementation of essentially non-oscillatory shock capturing schemes. *Journal of Computational Physics*, **77**, 439–471.

Sumer, B.M., Roulund, A., Fredsøe, J. and Michelsen, J. (2002). Three-dimensional numerical modeling of flow and scour around a pile. In: *Proc.,* 1*st International Conference on scour of foundations*, 795–809.

Sumer, B.M., Whitehouse, R.J.S. and Tørum, A. (2001). Scour around coastal structures: a summary of recent research. *Coastal Engineering*, **44**(2), 153 – 190.

Sutherland, J., Obhrai, C., Whitehouse, R.J.S. and Pearce, A.M.C. (2006). Laboratory tests of scour at a seawall. In: *3rd International Conference on Scour and Erosion, 3-5 July 2007, Gouda, The Netherlands.*

Ting, F.C.K. and Kirby, J.T. (1996). Dynamics of surf-zone turbulence in a spilling breaker. *Coastal Engineering*, **27**, 131–160.

Tsai, C.P., Chen, H.B. and You, S.S. (2009). Toe scour of seawall on a steep seabed by breaking waves. *Journal of Waterway, Port, Coastal, and Ocean Engineering*, **135**(2), 61–68.

van Rijn, L.C. (1984). Sediment transport, part I: Bed load transport. *Journal of Hydraulic Engineering*, **110**(10), 1431–1456.

Wilcox, D.C. (1994). *Turbulence modeling for CFD.* DCW Industries Inc., La Canada, California.

Wu, W., Rodi, W. and Wenka, T. (2000). 3D numerical modeling of flow and sediment transport in open channels. *Journal of Hydraulic Engineering*, **126**(1), 4–15.

Zou, Q., Peng, Z. and Lin, P. (2012). Effects of wave breaking and beach slope on toe scour in front of a vertical seawall. *Coastal Engineering Proceedings*, **1**(33), 122. ISSN 2156-1028.